Synthesis of zeolite X-carbon from coal bottom ash for hydrogen storage material

Nurul Widiastuti*, Mila Zhely Nurul Hidayah, Didik Praseytoko, Hamzah Fansuri

Chemistry Department, Institut Teknologi Sepuluh Nopember, Kampus ITS Sukolilo, Surabaya 60111, East Java, Indonesia

*Corresponding author. Tel: (+62) 087861137535; Fax: (+62) 0315928314; E-mail: nurul_widiastuti@chem.its.ac.id

ABSTRACT

Coal bottom ash is one of the solid wastes produced from coal combustion process in coal fired power station. The conversion of coal bottom ash into zeolite X-carbon was investigated in this research as an alternative method to reduce disposal cost or to minimize the environmental impact of the coal. Coal bottom ash was alkali fused using NaOH followed by hydrothermal at various time to produce zeolite X-carbon. The synthesized zeolite X-carbon was characterized using X-ray diffraction, scanning electron microscopy, and nitrogen adsorption. Hydrogen adsorption capacity was also determined. The crystalinity of the synthesized zeolite was found to change with hydrothermal time and the maximum value was obtained at hydrothermal temperature of $90^{\circ}C$ for hydrothermal time of 15 hours. The obtained zeolite X-carbon exhibits a high degree of crystalinity having BET surface area of 185.83 m^2/gram and a hydrogen sorption capacity of 1,66% wt at 30 °C/ 20 psi using gravimetric method. Copyright © 2014 VBRI press.

Keywords: Coal bottom ash; zeolite X-carbon; hydrogen storage materials.

Nurul Widiastuti is a senior lecturer in the Department of Chemistry, Institut Teknologi Sepuluh Nopember, Surabaya, Indonesia. She received. Her research interest is in development of zeolite, carbon and polymer composite materials for adsorption and membrane applications.

Hamzah Fansuri is a senior lecturer and the leader of materials for energy storge research group in the Department of Chemistry, Institut Teknologi Sepuluh Nopember, Surabaya, Indonesia. He leads research on membrane catalysts for methane to liquid conversion; conversion of methane, coal and biomass into syn gas and synthetic hydrocarbons; and fly ash geopolymerization and its applications.

Mila Zhely Nurul Hidayah was an undergraduate student in the Chemistry Department, Institut Teknologi Sepuluh Nopember, Surabaya, Indonesia. She has conducted research on porous materials such as zeolite and carbon for hydrogen storage.

Introduction

Coal is becoming the major source of Energy in Indonesia. According to the Indonesian Energy Mix Policy [1], coal will provide 33% of total domestic energy demand in 2025 compare to only 14% in 2006. As a result, there will be a tremendous increase of coal ash production, which will become a serious problem due to hazardous properties of the ash.

There are two kinds of coal ash, namely fly ash and bottom ash. Fly ash has been widely used as raw material in cement industries and building materials [2]. On the other hand, bottom ash has not been utilized and disposed of in a landfill and the bottom ash waste has become a pressing issue.

Bottom ash is generally composed of Si and Al in the form of aluminosilicate, as well as the unburnt carbon [3]. Converting bottom ash into zeolite-carbon material is one of the approaches to alleviate the disposal problem. Si and Al in the bottom ash act as raw materials for zeolite, whereas the unburnt carbon is a source of activated carbon. Excellent properties of zeolite and carbon can be found in zeolite-carbon materials. The composite material has hydrophilic surface with molecular level pores and high cation exchange capacity from the properties of zeolite. On the other hand, from the properties of carbon, the composite material has hydrophobic carbon surface with pores in the nanometer range and high surface area **[4].**

Thus composite is a promising material for hydrogen storage.

The use of zeolite for hydrogen storage material has been published [5,6]. It was reported that pore diameter of zeolite NaA, zeollite NaX and sodalit are 0.4, 0.74 and 0.43 nm, respectively, which is suitable for hydrogen molecule with kinetics diameter of 2.89 Å. Dong et al. [5] also compared the capacity of hydrogen adsorption of several type of zeolites namely, NaA, NaX, Na-LEV, H-OFF, Na-MAZ and Li-ABW. Results showed that zeolite-X has highest capacity for hydrogen adsorption, which achieved up to 1.74% (w/w) at pressure of 1.49 Mpa with surface area of 662 m3/g and pore volume of 0,36 ml/g.

Beside the zeolite, carbon material is also a potensial adsorbent for hydrogen storage [7]. Zhou, L et al. [8] reported that activated carbon revealed higher capacity in hydrogen storage compared to carbn nanotubes and carbon nanofibers. Activated carbon has pores with two or three times diameter of hydrogen molecule, which is optimum size for hydrogen storage [9]. In addition, specific surface area and micropore volume of carbon materials has a linear correlation with the hydrogen adsorption [10].

Based on the above discussion, it is, therefore, thought desirable to convert bottom ash to zeolite-carbon composite for hydrogen storage. However, the conversion process of zeolite-carbon from bottom ash could vary with the variety of coal sources. In this part of work, the condition of bottom ash conversion into zeolite-carbon is investigated. Further investigations on porous properties of the zeolite-carbon and its capacity in hydrogen storage are reported.

Experimental

Materials

The coal bottom ash was collected from PT. International Power Mitsui Operation and Maintenence Indonesia (IPMOMI), Paiton, Indonesia. The NaOH (p.a. $\geq$ 98%, pellets) and $NaAlO_2$ powder (contains 50-59% Al_2O_3 and 45% Na_2O) were purchased from Merck (UN 1283) and Sigma-Aldrich (UN 2812), respectively. The chemicals were of analytical grades and used without further purification, and demineralized water (aqua DM) was used during the synthesis process. Furthermore, the ultra-pure N_2 and H_2 gas (purity > 98%) which used during synthesis and characterization process were supplied from PT. Samator Gas Industry, Tangerang, Indonesia.

Preparation of bottom ash

The coal bottom ash was siftered until 60 mesh. Its water content was removed by heating at 110°C for 24 hours. The dried coal bottom ash was analyzed by X-ray Fluoresence (XRF PAN analytical PW4030), X-Ray Diffraction (XRD Philips MRD) and CHN-analyzer (LECO CHN-2000 Analyzer) to determine the chemical and mineralogical composition and carbon content of coal bottom ash.

Fusion bottom ash under N_2 atmosphere

The zeolite X-carbon composites were prepared using a two-step treatment, i.e. fusion followed by hidroternal treatment. The coal bottom ash was mixed with NaOH and then heated at 750°C for 1 hour in a tubular furnace. The

mass ratio between the ash and NaOH were 1:1.2. During the fusion process, N_2 gas was flown into the furnace through the sample in order to maintain unburned carbon content in bottom ash.

The product of fusion process was suspended into deionized water (12 ml/gram mass of product fusion) in polyethylene bottle followed by stirring and aging for 2 hours at room temperature. Subsequently, the solution was separated using a vacuum filtration equipment to separate the filtrate as the Si, Al and Na source from the solid precipitate containing the residual carbon as the carbon source for the synthesis.

Synthesis of zeolite X-carbon

Zeolite X-carbon composites were synthesized from the mixed solution and the carbon residue. The composition of the solution was controlled with molar ratio $NaAlO_2:SiO_2:NaOH: H_2O = 1:4:16:325$. The mixed solution was sealed in an autoclave reactor and then heated at 90°C with time variation of 8, 12, 15, 18 and 22 hours in order to determine the optimum crystallization time of the product. This hydrothermal treatment product was then separated by filtration, repeated washing using distilled water and drying at 105 °C for 24 hours.

Characterization

The resulting materials were examined using X-ray Diffraction (XRD) and Scanning Electron Microscope (SEM). The XRD data of samples were collected using Philips MRD X-ray Diffractometer with CuKα radiation (wavelength 1.54056 Å). SEM data of samples were collected using FEI type Inspect S50 Scanning Electron Microscope to confirm their surface morphology. The carbon content of samples were measured using LECO CHN-2000 analyzer. Futhermore, the specific surface area and porous textural characteristics of the composites were evaluated using Quantachrome gas adsorption analyzer. The specific surface area, micropore and mesopore characteristic were determined from the Brunauer-Emmet-Teller (BET), Saito-Foley (SF) and Barret Joyner Halenda (BJH) equations, respectively.

Hydrogen storage capacities

The hydrogen uptake experiment was performed at room temperature condition (25° - 30°C) and at relatively low pressure (20 psi). The zeolite X-carbon samples (around 5 gram) were dried at 110°C. The sample was then loaded into a sample holder which it was connected to an analytical balance's hook. Prior to the measurement, the sample was degassed at 350°C to remove undesired gases. The mass of the sample after degassing was recorded as the initial mass before hydrogen uptake measurement.

Hydrogen was then flown through the sample at 15 ml/min after which its hydrogen storage capacity was measured using the gravimetric method by observing changes of its weight. Hydrogen storage capacity test was performed until mass of the sample saturated. The mass of the sample was observed every 5-10 minutes and collected by Mettler Toledo MS 4002 SDR analytical balance. The amount of hydrogen uptake capacity was evaluated using Equation (1) [3],

$$\% H_2 = \frac{(m_1 - m_0)}{m_0} \times 100\% \qquad (1)$$

where m_0 is the initial mass of the sample, m_1 is the mass of the sample after the hydrogen uptake test and $\% H_2$ is the amount of the H_2 adsorbed on zeolite X-carbon (% wt.).

Results and discussion

Starting materials

The chemical composition of bottom ash is listed in **Table 1**. The main components for synthesis of zeolite-carbon composites such as SiO_2, Al_2O_3 and also unburned carbon are clearly dominating. Based on the XRD pattern, the main crystalline phases in this raw material are quartz (SiO_2) and mullite ($3Al_2O_3 \cdot 2SiO_2$), as shown in **Fig. 1 (a)**.

Table 1. Chemical composition of bottom ash.

Component	Content (mass%)
Si_2O_3	19.3
Al_2O_3	4.20
Fe_2O_3	48.9
CaO	22.8
K_2O	0.83
ZnO	0.18
MnO	0.51
Carbon	11.58
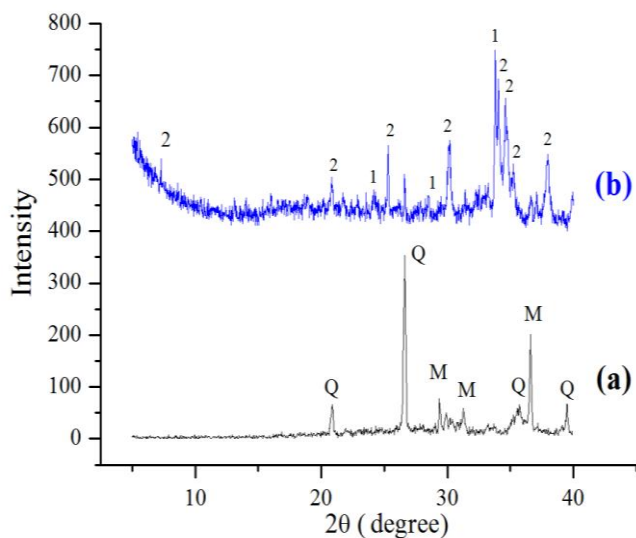
Fig. 1. XRD pattern of coal bottom ash (a) before and (b) after fusion treatment. (Q = quartz; M = mullite, 1= sodium silicate; 2 = sodium alumina silicate).

Fusion treatment of coal bottom ash

Fusion treatment resulted in the transformation of coal bottom ash into an amorphous material as shown by the broad hump in the XRD pattern at $2\theta = 5°\text{-}40°$ – see **Fig. 1(b)**. The dissapearance of crystalline phases during fusion treatment was due to their decomposition and dissolution with NaOH to form sodium silicate and sodium alumina silicate, as described in **Eq. (2) – (4)**:

$$2\ NaOH_{(s)} + Al_2O_{3\ (s)} \rightarrow 2\ NaAlO_{2\ (s)} + H_2O_{(g)} \qquad (2)$$

$$2\ NaOH_{(s)} + SiO_{2\ (s)} \rightarrow Na_2SiO_{3\ (s)} + H_2O_{(g)} \qquad (3)$$

$$10\ NaOH_{(s)} + 2\ SiO_2{\cdot}3Al_2O_{3\ (s)} \rightarrow \\ 2\ Na_2SiO_{3\ (s)} + 6\ NaAlO_{2\ (s)} + 5\ H_2O_{(g)} \qquad (4)$$
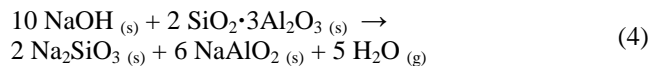
Dissolving further the fusion treatment product in deionized water (12 ml/grams mass of fusion product) resulted in the formation of solution sources of Na, Si and Al, as described in the following equations:

$$Na_2SiO_{3\ (s)} + H_2O_{(aq)} \rightarrow Na_2SiO_3 \qquad (5)$$

$$Na_2AlSiO_{4\ (s)} + H_2O_{(aq)} \rightarrow NaAl(OH)_{4\ (aq)} \qquad (6)$$

In the same solution, there was also an amount of precipitate solid of residual carbon, which could then be used as a carbon source for the synthesis of the zeolite-carbon composite.

Synthesis and characterization of zeolit X-carbon

The solution source and the residual carbon were mixed in the designated molar ratio to obtain a zeolite-carbon slurry. The formation of the zeolite X-carbon slurry is described in **Eq. (7):**

$$NaOH_{(aq)} + NaAl(OH)_{4(aq)} + Na_2SiO_{3(aq)} \xrightarrow{\text{Room Temp.}}$$

$$[Na_x(AlO_2)_y(SiO_2)_z{\cdot}NaOH{\cdot}H_2O]\ (gel) \xrightarrow{90°C} \qquad (7)$$

$$Na_p[(AlO_2)_p(SiO_2)_q]{\cdot}hH_2O\ (crystals)$$
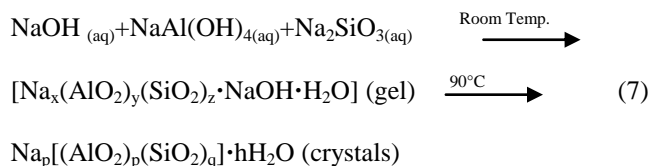
The slurry was converted into zeolite X-carbon composite with a good crystallinity by a hydrothermal treatment at 90°C, with varying treatment dwelling time. **Fig. 2** shows the XRD patterns of the resulting materials after the hydrothermal treatments. The patterns (based on **Fig. 2**) clearly indicate the presence of not only zeolite-X but also zeolite-A. The hump on the XRD pattern at $2\theta = 23°\text{–}35°$ indicates the coexistence of carbon and zeolites in an amorphous-crystalline mixture.

The presence of carbon decreases the crystallinity and purity of zeolite-X. Crystallinity of these resulting materials were calculated using **Eq.(8),** where the relative intensity of zeolite X-carbon were determined from the XRD data analysis.

$$\% \ Crystalinity = \frac{\Sigma Relative\ Int.of\ Zeolite\ X\text{-}carbon}{\Sigma Relative\ Int.of\ standard\ Zeolite\ X} \times 100\% \qquad (8)$$

Fig. 3 shows that the percentage degree of crystallinity of the zeolite X-carbon composite increases between 8 and 15 hours dwelling time, then decreases afterward. Indeed so because the surface structure of the materials is more regular after 8 to 15 hours treatment, but becomes irregular and complicated for longer treatment. From both XRD and SEM data, it can be concluded that the highest crystallinity

of zeolite in the composite sample was achieved at hydrothermal treatment of 90°C for 15 hours.
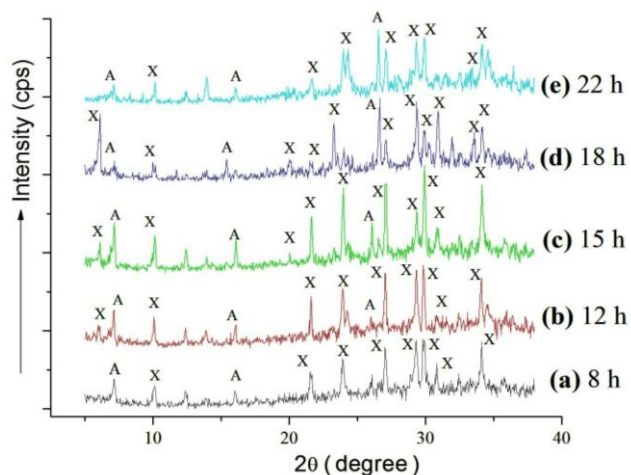
Fig. 2. XRD patterns of zeolite-carbon composite after fusion process followed by hydrothermal treatment at 90°C with various time.
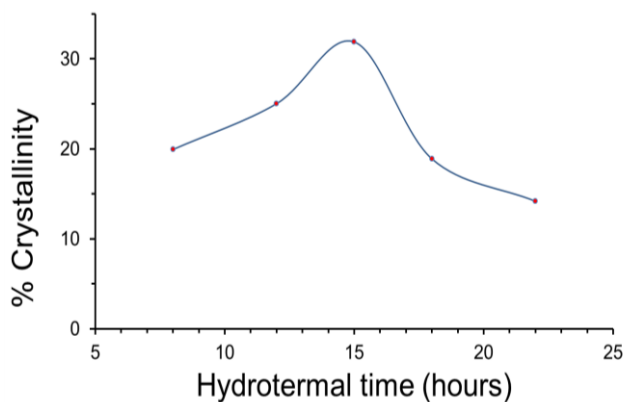
Fig. 3. Influence of hydrothermal treatment time toward the crystallinity of zeolite X-carbon prepared by hydrothermal treatment at 90°C.

Next, the development of zeolite X-carbon crystal shape through SEM analysis data was observed. Heat treatment for 8 hours initially produces zeolite-A, which shown as cubic crystals in **Fig. 4(a)**. After prolonged heat treatment, these cubics were developed into zeolite-X crystals (octahedral), which are indicated by the appearance of new shapes in some areas (**Fig. 4(b)** – **Fig. 4(c)**). This result is compatible with previous work **[11]**, which reported that zeolite-X was formed from overgrowth of zeolite A. However, heating the crystals up to 18-22 hours produced some irregular and complicated crystals, as shown in **Fig. 4(d)** – **Fig. 4(e)**. The SEM images shown in **Fig. 4** are in accordance with the XRD results on identifying zeolite-X as presented in **Fig. 2**.

In order to determine the uniformity of zeolite-X crystals formed on the surface of the activated carbon, a SEM analysis was performed with different magnifications. As shown in **Fig. 5**, the zeolite-X (octahedral) crystals are uniformly formed after 15 hours treatment. It is interesting to note that the size of the zeolite X-carbon aggregates correlates the amount of the activated carbon as can be observed from the elemental analysis results listed in **Table**

2. The larger aggregates (i.e., **Fig. 5 (a), (b)** and **(e)**) represent the larger the carbon content. Based on the characterization results, it can be concluded that zeolite X-carbon composites with good-crystallinity were successfully prepared by hydrothermal treatment at 90°C for 15 hours.
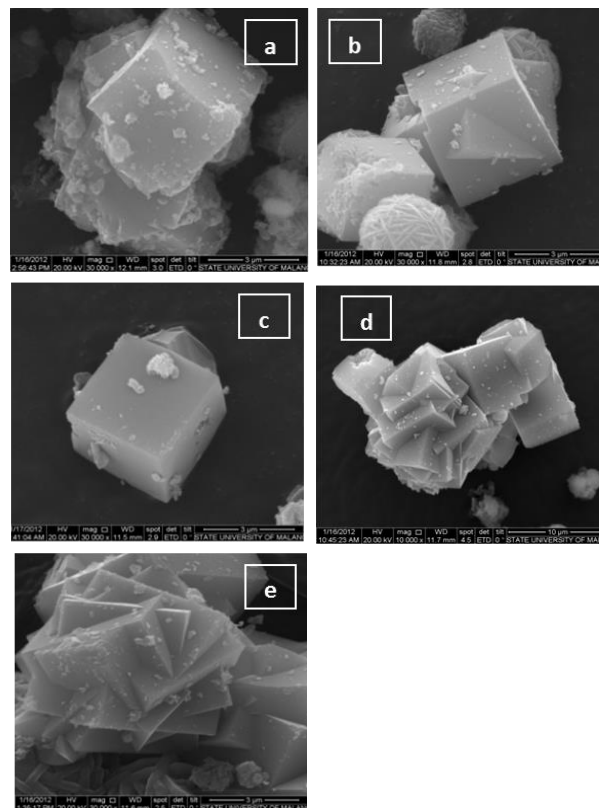
Fig. 4. SEM photographs of zeolite X-carbon prepared by hydrothermal treatment at 90°C for (a) 8 hours, (b) 12 hours, (c) 15 hours, (d) 18 hours dan (e) 22 hours.

Pore characteristics of the zeolite X-carbon

The pore characteristics and the surface area of the zeolite X-carbon prepared with optimum hydrothermal conditions (90°C, 15 hours) were investigated by N_2 adsorption analysis. The surface area of the zeolite X-carbon composites as measured using BET (**Eq.(9)**) is plotted as shown in **Fig. 6**.

$$\frac{1}{W\left(\left(\frac{P_0}{P}\right)-1\right)} = \frac{1}{W_m C} + \frac{C-1}{W_m C}\left(\frac{P_0}{P}\right) \tag{9}$$

Table 2. Carbon content of zeolite X-carbon resulting materials.

No.	Sample	Carbon content (%mass)
1.	Coal bottom ash	11.58
2.	Zeolite X-carbon 90° (8 hours)	5.05
3.	Zeolite X-carbon 90° (12 hours)	5.08
4.	Zeolite X-carbon 90° (15 hours)	4.52
5.	Zeolite X-carbon 90° (18 hours)	4.63
6.	Zeolite X-carbon 90° (22 hours)	4.84
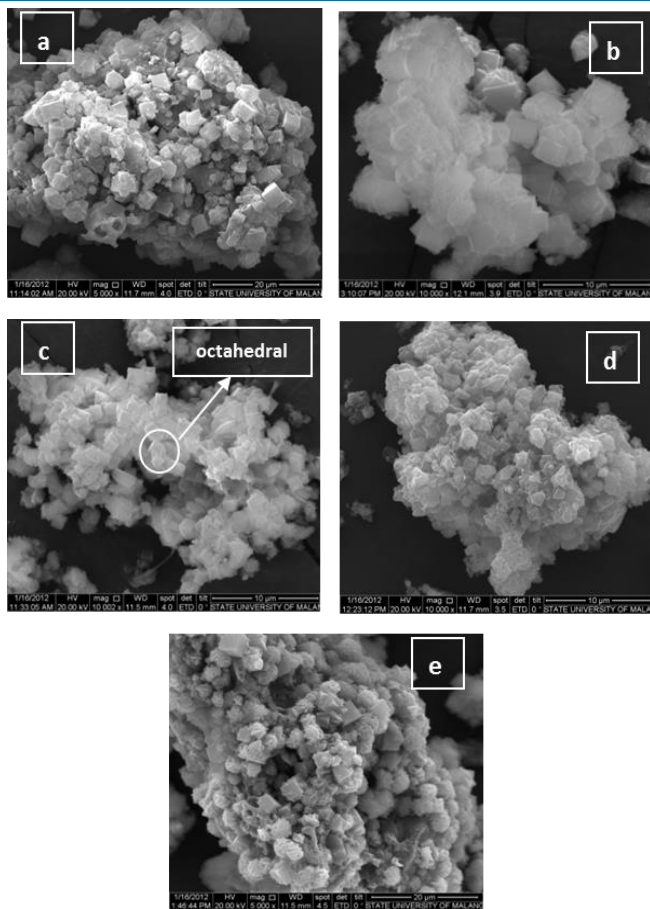
Fig. 5. SEM photographs of zeolite X-carbon composites prepared by hydrothermal treatment at 90°C for (a) 8, (b) 12, (c) 15, (d) 18 and (e) 22 hours.

Clearly, the evolution of zeolite X-carbon sample on adsorption isotherms as P/P_0 can be described as a Type-IV isotherm with a characteristic hysteresis and is often associated with mesopores (diameter 2 – 100 nm) according to IUPAC **[12]**. The observed hysteresis between P/P_0 of 0.4 and 1 is attributed to the capillary condensation and is normally due to the presence of mesopores **[12]**. In a previous work **[13]**, this hysteresis was also asserted to indicate cylindrically shaped pores. **Table 3** lists the textural properties of zeolite X-carbon, in order to understand the pore structures of the zeolite X-carbon in detail.

Generally, a zeolite has a pore diameter of approximately 0.65 to 1.18 nm **[6,14]**. However, in this work, the zeolite X-carbon has a larger pore diameter up to 3 nm. Larger pore diameter is due to the presence of carbon, which has been activated during the hydrothermal treatment, thus also resulting relatively high surface areas **[15]**.

Hydrogen uptake capacities

In this work, the selected zeolite X-carbon composite were also examined for its hydrogen uptake capacities using gravimetic method following **Eq.(1). Fig. 7** shows the hydrogen storage capacities of the composite. The capacity continuously increases up to 90 mins and then levels-off

afterward, implying that it exhibits hydrogen uptake saturation after 90 mins.
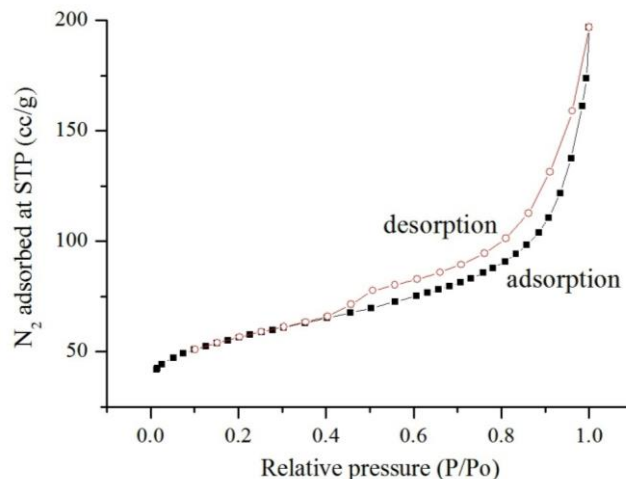
Fig. 6. N_2 adsorption/desorption isotherms of zeolite X-carbon prepared by hydrothermal treatment at optimum condition (90°C for 15 hours).

Table 3. Pore characteristic and surface area of zeolite X-carbon.

Parameter	Results	Calculated by
Surface areas	185.824 m²/gram	BET
Mesopore	Pore diameter = 3 nm	BJH
	Pore volume = 0.2 cc/gram	
Micropore	Pore diameter = 0.34 nm	SF
	Pore volume = 0.068 cc/gram	

The average hydrogen uptake capacities of zeolite X-carbon after several measurements was up to 1.66 % wt. This figure is larger than that of pure zeolites, which was reported between 0.4 % wt. and 0.9 % wt. at 30 °C/100 bar **[16,17],** but smaller than that of activated carbon, which was reported up to 3% wt. at 298 K/100 bar **[18].** The larger capacity of the zeolite X-carbon composite as compared to the zeolite X can be attributed to the presence of the carbon, which improves the pore characteristics of the zeolite X and causes a relatively high surface area and well-developed pore characteristics.
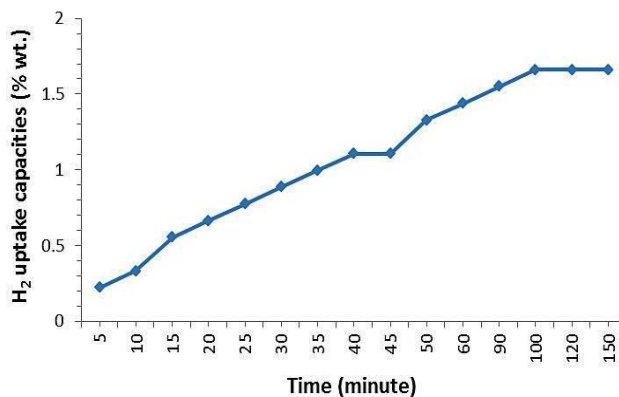
Fig. 7. Hydrogen uptake capacities of zeolite X-carbon, which prepared by hydrothermal treatment in optimum condition (90°C for 15 hours).

Conclusion

Bottom ash was successfully converted into zeolite X-carbon composites by a combined processs of fusion and hydrothermal treatment.   Based on the results, hydrothermal time has an effect on the zeolite-X crystallinity and the amount of carbon content of the zeolite-carbon composites. The composite with best zeolite-X crystallinity has been successfully synthesized from coal bottom ash by fusion treatment followed by hydrothermal treatment at 90°C for 15 hours. Irregular crystal of zeolite-X was found after hydrothermal time of 22 hours. The zeolite-composite with best crystallinity ha surface area of 185.824 m2/gram and micro- as well as meso-pore diameters of 0.34 nm and 3 nm, respectively. Hydrogen uptake of the composite was up to 1.66 % wt. at 30 °C/20 psi. These characteristics indicate that the composite is suitable for hydrogen storage application.

Reference

1. Kelompok Kajian Kebijakan Mineral dan Batubara, **2006**. http://www.tekmira.esdm.go.id/data/files/Batubara%20Indonesia.pdf
2. Querol, X.; Moreno, N.; Umana, I. C.; Alastuey, A.; Hernandez, E.; *Int. J. Coal Geo.l*, **2002**, 50, 413.
   DOI: 10.1016/S0166-5162(02)00124-6
   Shoude, W.; Lingchao, L.; Xin, C. *Advanced Materials Letters*, **2011**, *2*, 12.
   Amaladhas, T.P.; Thavamani, S.S. *Advanced Materials Letters*, **2013**, *4*, 213.
3. Chang , F. Y.; Wey, M. Y.; *J. Hazard. Mater.*, **2006**, 138, 594.
   DOI: 10.1016/j.jhazmat.2006.05.099
   Kondawar, S.B.; Dahegaonkar, A. D.; Tabhane, V. A.; Nandanwar, D. V. *Advanced Materials Letters*, **2014**, *5*, 360.
4. Gao, N.F.; Kume, S.; Watari, K.; *Mat. Sci. Eng. A,* **2005,** 404, 274.
   DOI: 10.1016/j.msea.2005.05.090
   Amaladhas, T.P.; Thavamani, S.S. *Advanced Materials Letters*, **2013**, *4*, 688.
5. Dong, J. X.; Wang, X.; Xu, H.; Zhao, Q.; Li, J.; *Int. J. Hydrogen Energ.*, **2007**, 32, 4998.
   DOI: 10.1016/j.ijhydene.2007.08.009
   Tiwari, A.; Shukla, S.K. (Eds.), In Advanced Carbon Materials and Technology, John Wiley & Sons, USA, **2013**.
6. Langmi, H. W.; Walton, A.; Al-Mamouri, M. M.; Johnson, S. R.; Book, D.; Speight, J. D.; Edwards, P. P.; Gameson, I.; Anderson, P. A.; Harris, I. R.; *J. Alloy. Compd.*, **2003**, 356–357, 710.
   DOI: 10.1016/S0925-8388(03)00368-2
7. Kopac, T.; Toprak, A.; *Int. J. Hydrogen Energ.*, **2007**, 32, 5005.
   DOI: 10.1016/j.ijhydene.2007.08.002
   Tiwari, A.; Valyukh, S. (Eds.), In Advanced Energy Materials, John Wiley & Sons, USA, **2014**.
8. Zhou, L., Zhou, Y., Sun, Y.; *Int. J. Hydrogen Energ.,* **2004**, 29, 475.
   DOI: 10.1016/S0360-3199(03)00092-2
9. Huang, C.; Chen, H.; Chen, C.; *Int. J. Hydrogen Energ.*, **2010**, 35, 2777.
   DOI: 10.1016/j.ijhydene.2009.05.016
10. Texier-Mandoki, N.; Denntzer, J.; Piquero, T.; Saadallah, S.; David, P.; Vix-Guterl, C.; *Carbon*, **2004**, 42, 2744.
    DOI: 10.1016/j.carbon.2004.05.018
11. Porcher, F.; Dusausoy, Y.; Souhassou, M.; Lecomte, C.; *Min. Mag.*, **2000**, 64, 1.
    DOI: 10.1180/002646100549012
12. Sing, S. K. W; Gregg, S. J.; Adsorption, Surface Area and Porosity. Second Edition, Academic Press: New York, **1982**, p. 321.

ISBN: 0123009561.
13. Lee, S. Y.; Park, S. J.; *Int. J. Hydrogen Energ.*, **2010**, 35, 6757.
    DOI:10.1016/j.ijhydene.2010.03.114
14. Weitkamp, J.; Fritz, M.; Ernst, S.; *Int. J. Hydrogen Energ.*, **1995**, 20, 967.
    DOI: 10.1016/0360-3199(95)00058-L
15. Katsuki, H; Komarneni, S.; *J. Solid State Chem.,* **2009**, 182, 1749.
    DOI: 10.1016/j.jssc.2009.04.022
16. Chung, K. H.; *Energy,* **2010**, 35, 2235.
    DOI: 10.1016/j.energy.2010.02.010
17. Li, J.; Wu, E.; *J. Supercrit. Fluid.,* **2009**, 49, 196.
    DOI: 10.1016/j.supflu.2008.12.015
18. Ströbel, R.; Garche, J.; Moseley, P. T.; Jörissen, L.; Wolf, G. *J. Power Sources*, **2006**, 159, 781.
    DOI: 10.1016/j.jpowsour.2006.03.047